JGR Space Physics

RESEARCH ARTICLE
10.1029/2022JA030570

Interaction Between Proton Aurora and Stable Auroral Red Arcs Unveiled by Citizen Scientist Photographs

Y. Nishimura[1], E. Bruus[2], E. Karvinen[3], C. R. Martinis[4], A. Dyer[5], L. Kangas[2], H. K. Rikala[6], E. F. Donovan[7], N. Nishitani[8], and J. M. Ruohoniemi[9]

[1]Department of Electrical and Computer Engineering and Center for Space Physics, Boston University, Boston, MA, USA, [2]Taivaanvahti/Skywarden Observation Service, Ursa Astronomical Association, Helsinki, Finland, [3]Citizen Scientist, Nurmes, Finland, [4]Department of Astronomy and Center for Space Physics, Boston University, Boston, MA, USA, [5]Citizen Scientist, Strathmore, AB, Canada, [6]Citizen Scientist, Valtimo, Finland, [7]Department of Physics and Astronomy, University of Calgary, Calgary, AB, Canada, [8]Institute for Space Earth Environmental Research, Nagoya University, Nagoya, Japan, [9]Bradley Department of Electrical and Computer Engineering, Virginia Tech, Blacksburg, VA, USA

Key Points:

- Citizen scientist photographs revealed a peculiar evolution of subauroral emission during substorms
- Initial red and green emissions were identified as proton aurora by secondary electrons
- The transition from proton aurora to a SAR arc was found. Proton aurora gives evidence of proton injection as initiation of the SAR arc

Correspondence to:
Y. Nishimura,
toshi16@bu.edu

Citation:
Nishimura, Y., Bruus, E., Karvinen, E., Martinis, C. R., Dyer, A., Kangas, L., et al. (2022). Interaction between proton aurora and stable auroral red arcs unveiled by citizen scientist photographs. *Journal of Geophysical Research: Space Physics*, *127*, e2022JA030570. https://doi.org/10.1029/2022JA030570

Received 19 APR 2022
Accepted 21 JUN 2022

Abstract We utilized citizen scientist photographs of subauroral emissions in the upper atmosphere and identified a repeatable sequence of proton aurora and subauroral red (SAR) arc during substorms. The sequence started with a pair of green diffuse emissions and a red arc that drifted equatorward during the substorm expansion phase. Simultaneous spectrograph and satellite observations showed that they were subauroral proton aurora, where ion precipitation created secondary electrons that illuminated aurora in green and red colors. The ray structures in the red arc also indicated existence of low-energy electron precipitation. The green diffuse aurora then decayed but the red arc (SAR arc) continued to move equatorward during the substorm recovery phase. This sequence suggests that the SAR arc was first generated by secondary electrons associated with ion precipitation and may then transition to heat flux or Joule heating. Proton aurora provides observational evidence that ion injection to the inner magnetosphere is the energy source for the initiation of the SAR arc.

Plain Language Summary Photographs that were taken by citizen scientists at Strathmore (Canada), Orimattila (Finland) and Ikaalinen (Finland) revealed peculiar green bands and blobs and red arcs in the night sky equatorward of the auroral oval. Those are different from STEVE (Strong Thermal Emission Velocity Enhancement) due to the lack of the purple/mauve arc and green picket fence. Using concurrent scientific instruments, we identified that those are a type of proton aurora that is illuminated by electrons induced by proton precipitation from space. The proton aurora transitions to a stable auroral red (SAR) arc. A series of photographs suggests that the SAR arc is initiated by proton precipitation, which has been suggested but never been demonstrated previously. The citizen scientist photographs played a critical role in unveiling the interaction between the proton aurora and SAR arc.

1. Introduction

Recently, a growing number of citizen scientists post photographs of the night sky, and they have made important contributions to shed light on upper atmospheric emissions that were little known among scientists. Citizen scientists brought Strong Thermal Emission Velocity Enhancement (STEVE) (MacDonald et al., 2018) to scientists' attention, and their photographs were an essential piece for recognize its existence and distinction from previously known types of emissions in the upper atmosphere. Dunes (Palmroth et al., 2020) are another discovery of upper-atmospheric emissions that was achieved by citizen scientist photographs. The present work was also motivated by citizen scientist photographs at subauroral latitudes in three nights. Observations indicate that the optical emissions resemble proton aurora and stable auroral red (SAR) arcs, but interestingly, the emissions show a dynamic interplay between the two types of phenomena that to our knowledge has never been reported.

Proton aurora is caused by energetic proton precipitation from the ring current in the inner magnetosphere (Egeland & Burke, 2019). Proton aurora in terms of ground-based observations often refers to H_β (486.1 nm) emissions, but proton precipitation also creates secondary electrons, whose collision with neutrals emits green (557.7 nm) light. The green emission is much brighter than the H_β line, and proton aurora is recognized as green diffuse aurora in naked eyes (Ono et al., 1987). Proton aurora occasionally includes red (630.0 nm) emissions (Lummerzheim et al., 2001; Sakaguchi et al., 2012), and secondary electrons are also considered as the source of the red color in proton aurora.

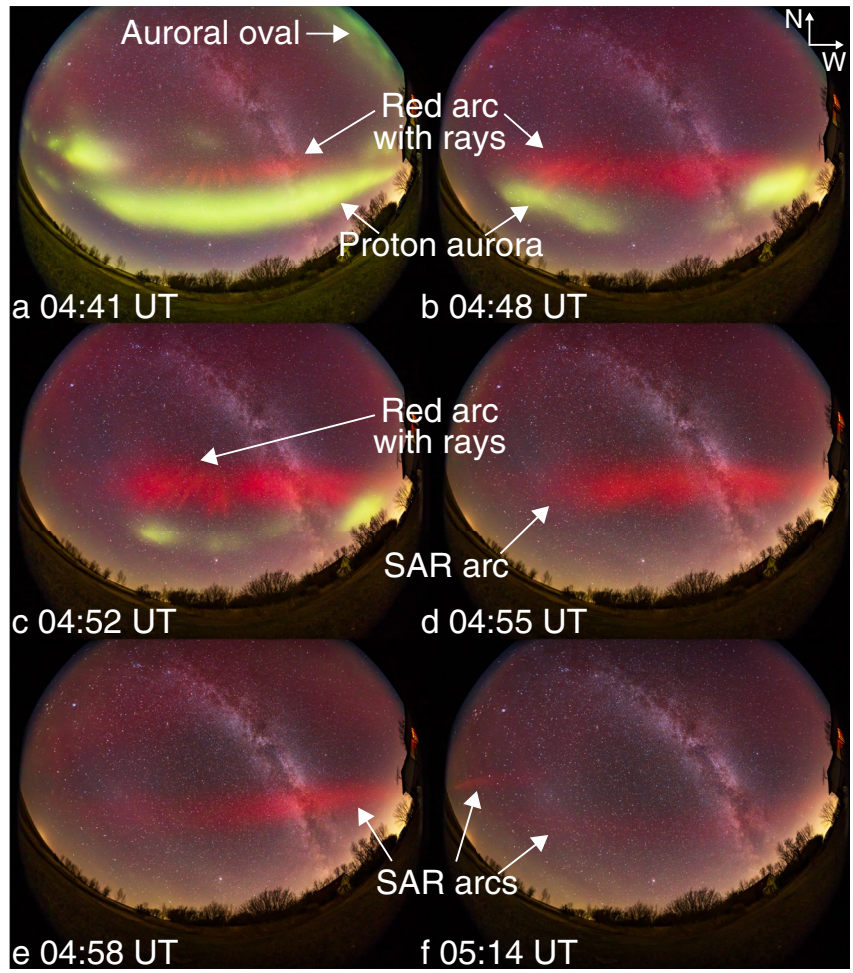

Figure 1. Green diffuse aurora and SAR arc that were observed at Strathmore, Canada on 12 October 2021. North is to the top and west is to the right. The exposure is between 13 and 15 s.

In contrast, SAR arcs are dominated by emissions at the 630.0 nm wavelength, and they generally do not involve other wavelengths (with an exception of a rare event (Mendillo et al., 2016)). SAR arcs also lack proton or electron precipitation (Foster et al., 1994), and thermal heat fluxes from the inner magnetosphere have been considered as the source of emission (Gallardo-Lacourt et al., 2021).

Both proton aurora and SAR arcs occur during geomagnetically disturbed times (storms and substorms) (Gallardo-Lacourt et al., 2021). Energetic ions are injected from the magnetotail to the inner magnetosphere during those times, and become a source of energy. Proton aurora is caused by energetic ions that are scattered by electromagnetic ion cyclotron waves and precipitate to the upper atmosphere. Energetic ions also heat ambient cold plasma (plasmasphere), and heated thermal electrons are believed to cause SAR arcs (Inaba et al., 2021). Proton aurora occurs near the meridian of intensifications in the auroral oval (streamers) (Henderson, 2021; Montbriand, 1971; Nishimura et al., 2014). SAR arcs detach from the auroral oval during substorms (Oyama et al., 2020; Takagi et al., 2018)

Although both proton aurora and SAR arcs are related to ion injections to the inner magnetosphere, proton aurora and SAR arcs have been investigated separately, and to our knowledge, there has been no report about the relation between proton aurora and SAR arcs. Moreover, despite that energetic ions are the energy source of SAR arcs, SAR arcs have never been reported with ion precipitation.

Using citizen scientist photographs and scientific instruments (imagers and low-altitude satellites), we present that the SAR arcs are preceded by proton aurora during substorms. Interaction between the proton aurora and SAR arc

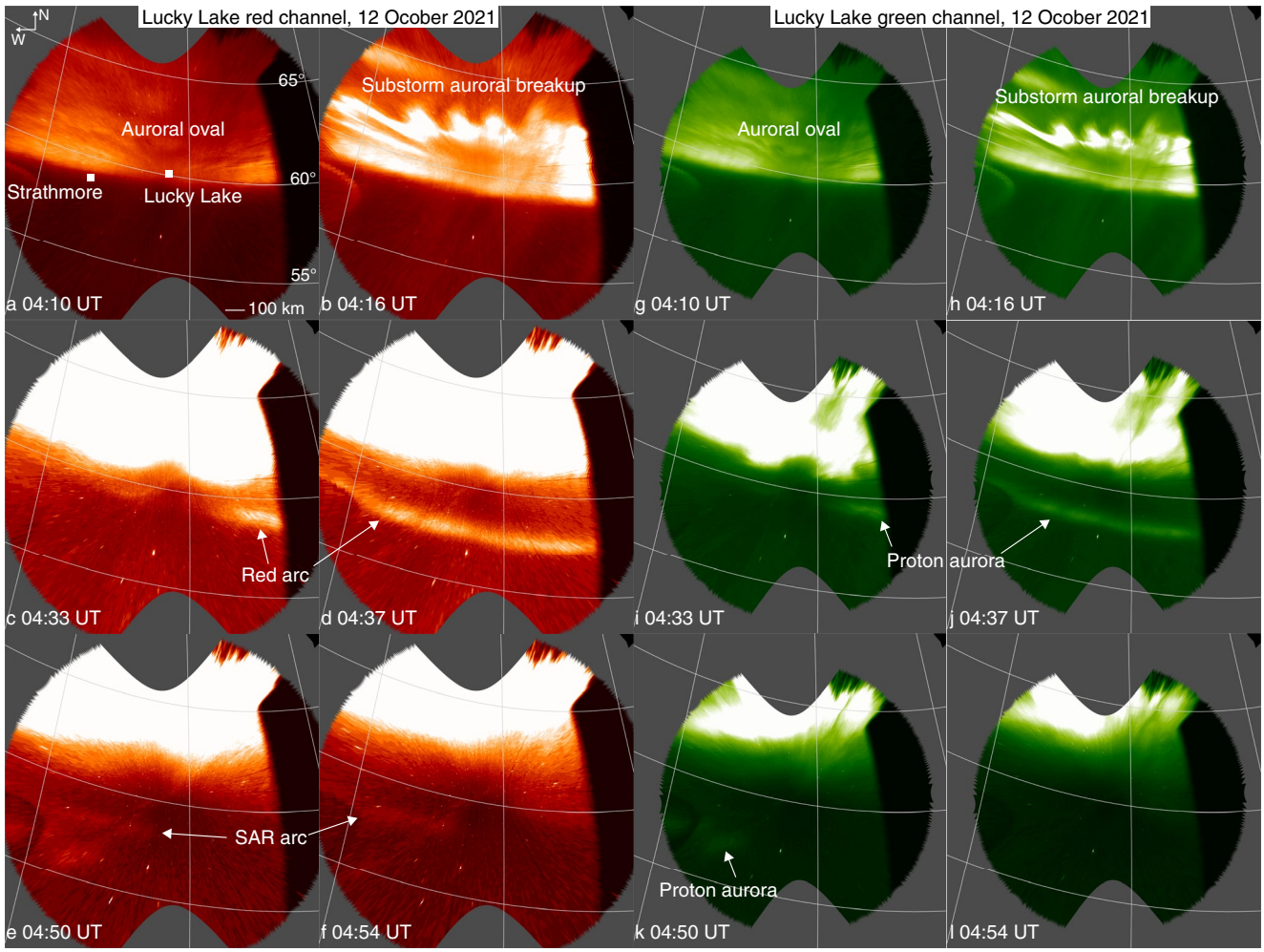

Figure 2. Selected snapshots of all-sky imager data at Lucky Lake, Canada in (left) red and (right) green color channels.

suggests that secondary electrons associated with ion precipitation initiate the SAR arc. The existence of proton aurora also provides observational evidence that proton injection to the inner magnetosphere is the source for the SAR arc.

2. Results and Discussion

2.1. 12 October 2021 Event

Figure 1 shows selected citizen-scientist photographs taken at Strathmore, Canada between 04:41 and 05:14 universal time (UT), at 58.6° magnetic latitude (MLAT) between 20.5 and 21.0 hr magnetic local time (MLT). The auroral oval was located near the northern horizon, and much of the field-of-view (FOV) covered subauroral latitudes. Distinct features in the beginning of the event sequence are a red arc and green diffuse bands and blobs that were approximately aligned in the east-west direction (Figure 1a). The green diffuse bands and blobs did not have clear internal structure, while the red arc had ray structure. The green diffuse emission subsided and disappeared within 13 min from the first photograph (Figures 1b–1d). The red arc lasted for another 20 min (Figures 1e and 1f). The lack of other emission colors indicates that this is a SAR arc, and the SAR arc did not show ray structures. Another SAR arc appeared northwest of the existing SAR arc near the end of the event sequence (Figure 1f). This event does not involve a purple/mauve arc or a picket fence, and thus is different from STEVE.

The Transition Region Explorer (TREx) true color imager at Lucky Lake, Canada (59.8° MLAT between 21.0 and 21.5 hr MLT) (Gillies et al., 2020) is located near Strathmore and provided observations over a longer time interval. Figure 2 shows selected snapshots of data at the red and green channels that were projected to the sky

at 230 (red) and 110 (green) km altitude. The equatorward boundary of the auroral oval was located at 59°-60° MLAT, and the subauroral region did not show any optical emission (Figures 2a and 2b). The equatorward boundary was located near the zenith of the imager, and thus its latitude has little uncertainties. A substorm auroral breakup occurred at ~04:13 UT (Figures 2c and 2d). It includes a wavy structure known as beads, which are characteristic to substorm onset (Donovan et al., 2006; Nishimura et al., 2016). Then the red arc and green diffuse aurora appeared near the equatorward edge of the auroral oval and moved southwestward (Figures 2e–2h). The red and green emissions were located at the same horizontal positions in the sky, indicating that the emissions had a common energy source. Then the green emission faded and only the SAR arc remained in the FOV (Figures 2i and 2j).

The TREx spectrograph at Lucky Lake (Gillies et al., 2020) measured emission spectra along the north-south meridian, and provided important information for identifying the nature of the emissions. The green line (557.7 nm) emission was observed just equatorward of the auroral oval (equatorward of the dashed line) during the substorm expansion phase at 04:34-04:47 UT, and it overall moved equatorward (Figures 3a and 3c). This emission corresponds to the ones in Figure 1 is thus of our interest. The green line emission was associated with the H_β line (486.1 nm). Blue line (427.8 nm) emissions were also present, but the blue-to-green ratio was much lower than that in the auroral oval. Hence, this emission is not created by plasma sheet electrons. Considering that the emissions were located in the subauroral ionosphere, this is subauroral proton aurora. Although the H_β line is dim, proton aurora is brightest at the green line due to secondary electrons that are induced by primary proton precipitation from the inner magnetosphere (Ono et al., 1987). Note that proton aurora was also present in the auroral oval. Electron aurora, however, is very bright in the auroral oval, and contributions of the proton aurora in the auroral oval are minor.

The red line (630.0 nm) emission in the proton aurora can also be explained by the secondary electrons, when the secondary electrons have sufficiently high fluxes at low energies (Lummerzheim et al., 2001). A major difference from the other spectral lines is that the red line emission lasted for at least 30 min after the decay of the proton aurora (i.e., SAR arc) and continued to move equatorward. The emergence of a SAR arc during a substorm has been known through past observations (Takagi et al., 2018), but a unique feature in the present observations is that the initiation of the red line emission coincides with the proton aurora. The coexistence of the proton aurora and red arc in Figures 1 and 2 suggests that the initial red emission is created by secondary electrons that were created by proton precipitation. The ray structure in Figures 1a–1c is analogous to the patches of emission along the SAR arc (Mendillo et al., 2016). The elevation of their SAR arc was too low to examine a relation to proton aurora, but the present observations revealed the emission structure across all altitudes.

The proton aurora and SAR arc also coincided with subauroral polarization streams (SAPS). The subauroral flow speed increased during the substorm expansion phase, and decayed during the recovery phase. Collisional heating and heat conduction could also be a source of the 630.0 nm emission.

The Defense Meteorological Satellite Program (DMSP)-17 satellite was located in the southern hemisphere magnetically conjugate to the Lucky Lake imager FOV (Figure 4a) at 04:50–04:54 UT. The DMSP observations confirm that the region of interest (after 04:52 UT) had the ionospheric trough, SAPS flow, electron heating, and downward field-aligned currents (FACs, Figures 4b–4e), and this region did not have any energetic electron precipitation. The flow after 04:52:20 UT was anti-sunward, and it is consistent with a brief anti-sunward flow in the Super Dual Auroral Radar Network (SuperDARN) observations (Figure 3f). Except for the anti-sunward flow, the other features in Figures 4b–4e are consistent with past satellite observations of the SAR arc (Foster et al., 1994). A weak ion precipitation was observed at 04:52:40 UT, near the end of the proton aurora (Figure 4g). The energetic ion precipitation validates the presence of the proton aurora. A weak electron precipitation was also seen below ~200 eV (Figure 4f). Although the low-energy electron flux at the satellite altitude (~830 km) was not sufficiently high to create visible emission, the low-energy electron flux may indicate that secondary electrons began to form above the satellite altitude and may have a higher flux at lower altitude as precipitating ions collide more with neutrals.

2.1.1. 07 April 2016 Event

Figure 5 shows selected citizen-scientist all-sky images that were taken at Orimattila, Finland between 20:00 and 22:31 UT on 07 April 2016 (57.0° MLAT between 22.3 and 0.8 hr MLT). This event shows essentially

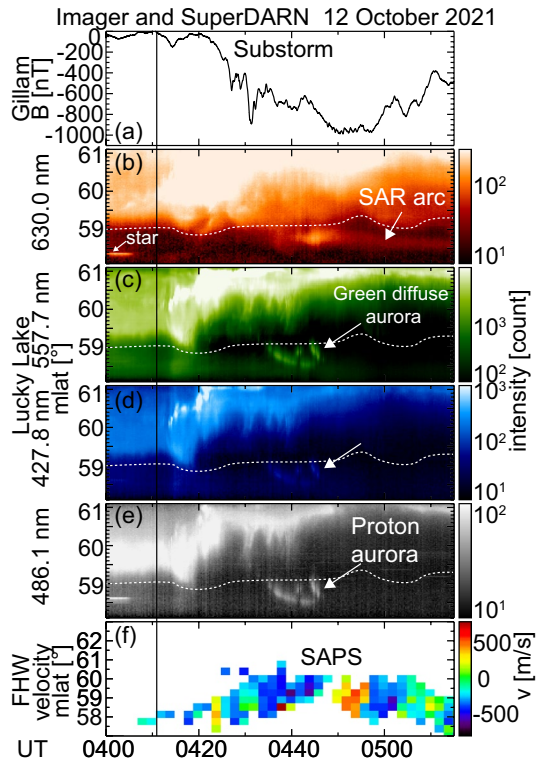

Figure 3. *H*-component of ground magnetometer data at Gillam, spectrograph data at Lucky Lake at 630.0, 557.7, 427.8 and 486.1 nm, and SuperDARN Fort Hays West (FHW) line-of-sight velocity. The dashed line marks the equatorward boundary of the auroral oval at 630.0 nm.

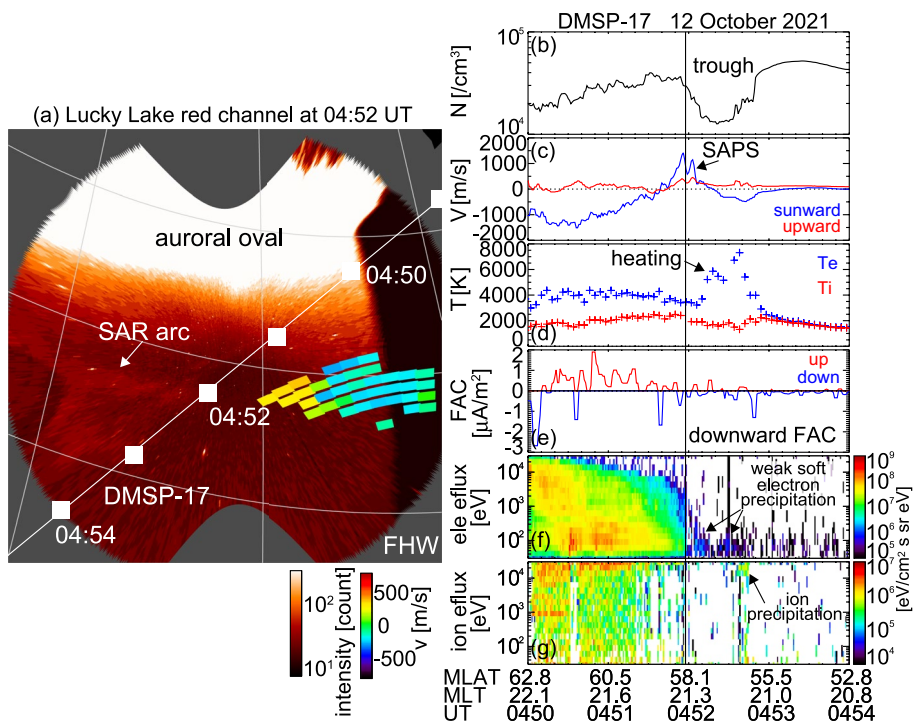

Figure 4. (Left) Snapshot of all-sky imager data at 04:52 UT and the footprint of the DMSP-17 satellite. Snapshot of SuperDARN Fort Hays West velocity data. (Right) DMSP-17 measurements of the density, velocity, temperature, field-aligned current (FAC), electron flux, and ion flux.

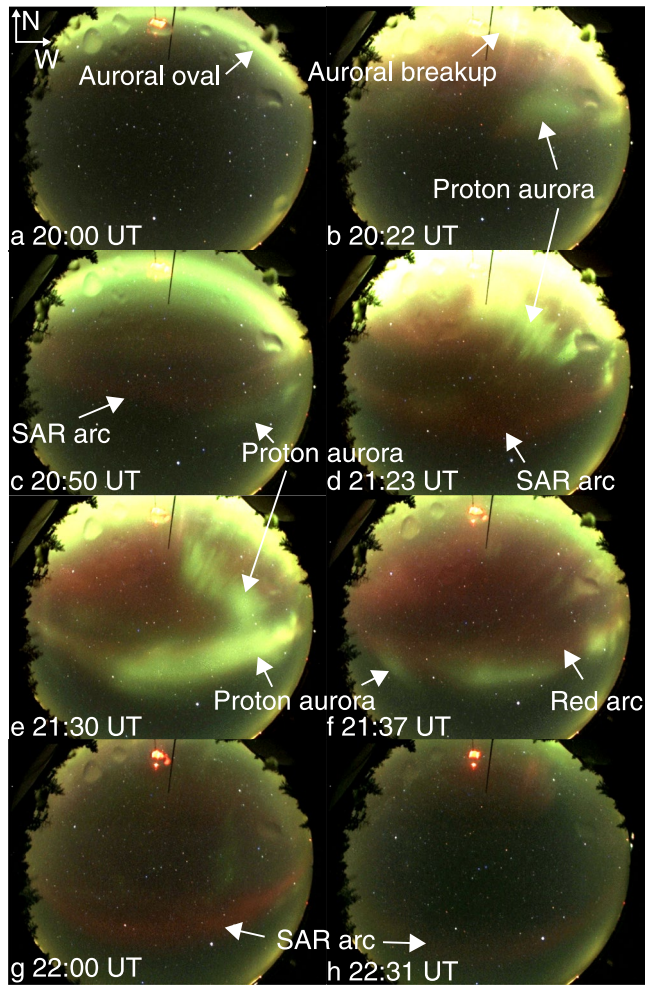

Figure 5. Green diffuse aurora and SAR arc that were observed at Orimattila, Finland on 07 April 2016. North is to the top and east is to the left. The image cadence is 1 min.

the same event sequence as the first event, but the sequence occurred multiple times. A substorm auroral breakup occurred, and green diffuse aurora appeared equatorward of the auroral oval (Figure 5b). The green diffuse aurora was associated with a red arc. The green diffuse aurora decayed but the red arc lasted longer (SAR arc, Figure 5c). In this event, the event sequence repeated three times (Figure 6). The second green diffuse aurora and red arc started around 20:50 UT, and the third and strongest green diffuse aurora and red arc started around 21:20 UT (Figure 5d). In each event sequence, the green diffuse aurora and red arc moved equatorward as an azimuthally narrow channel, and then formed azimuthally elongated green bands or blobs (Figures 5d and 5e). The red arc appeared in the same region and then only the red arc remained (SAR arc, Figures 5g, 5h and 6b).

The MetOp-02 satellite was in conjunction with the green and red emissions near the western edge of the images that were mapped to the sky (Figures 7a and 7b). The green emission was associated with proton precipitation (Figures 7c and 7d) equatorward of the auroral oval (after 20:21:30 UT). This is consistent with the first event and supports that proton precipitation is the primary driver of the emission.

2.1.2. 04 November 2018 Event

The third event occurred at 18–20 UT on 04 November 2018. Figure 8 shows a series of citizen-scientist photographs that were taken at Ikaalinen, Finland. The event sequence was essentially the same as those in the other events: Green diffuse auroral bands and blobs appeared equatorward of the auroral oval (Figure 8a), and then a red arc emerged near (Figures 8b and 8d) and on (Figure 8c) the green emission. The green emission faded away

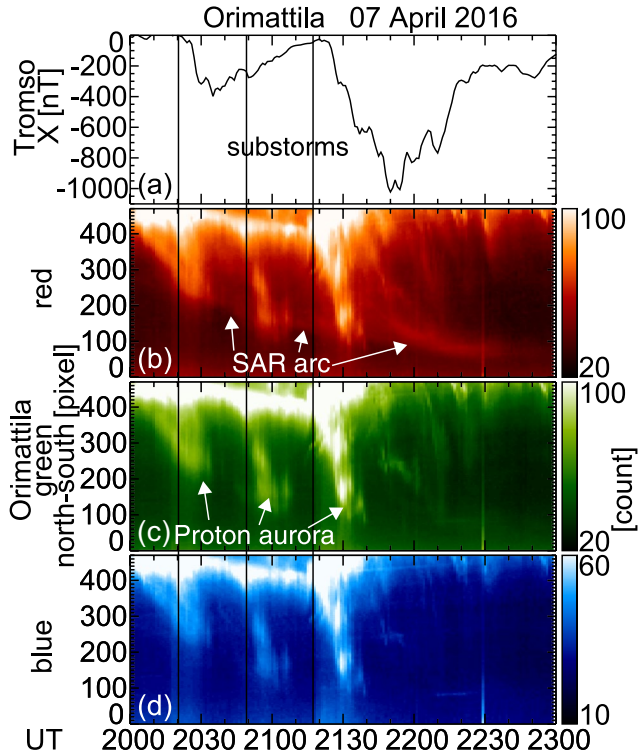

Figure 6. *H*-component of ground magnetometer data at Tromso, and the red, green and blue channels of the all-sky images.

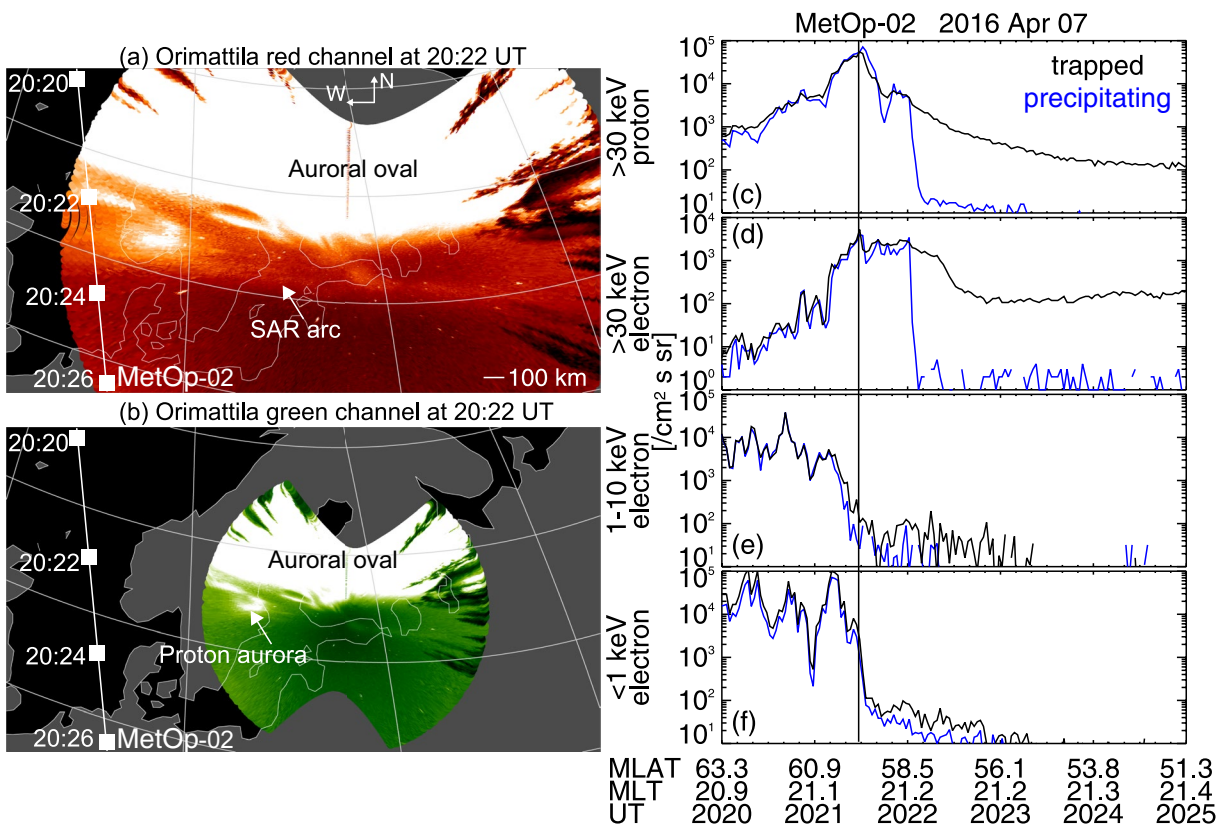

Figure 7. (Left) Snapshot of all-sky imager data in the red and green channels at 20:22 UT and the footprint of the MetOp-02 satellite. (Right) MetOp-02 measurements of the >30 keV proton, >30 keV electron, 1–10 keV electron, and <1 keV electron fluxes.

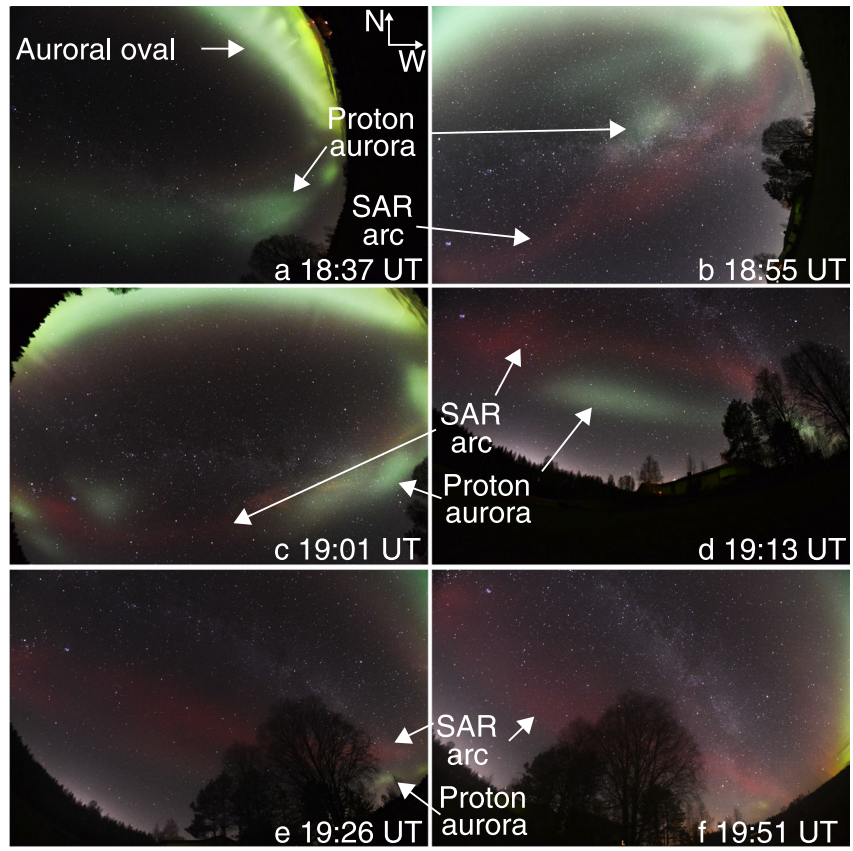

Figure 8. Green diffuse aurora and SAR arc that were observed at Ikaalinen, Finland on 4 November 2018. North is to the top and east is to the left. The exposure is between 13 and 30 s.

except near the western horizon, and the red arc persisted as a SAR arc (Figures 8e and 8f). This event was also associated with a large substorm that started near 18:20 UT (AL ~ −900 nT, not shown). The photographs for this event were only taken intermittently, and we do not have sufficient data to create keograms.

The MetOp-02 satellite was in conjunction with the green and red emissions near the center of the images that were mapped to the sky (Figures 9a and 9b). Similar to the satellite observations in the other two events, the green emission was associated with a distinct enhancement of proton precipitation (Figure 9c) equatorward of the auroral oval (after ~18:59 UT). The >30 keV proton precipitation is a typical signature of electron scattering by electromagnetic ion cyclotron (EMIC) waves (Nishimura et al., 2014). While 1–10 keV electron precipitation was negligibly small, the <1 keV electron fluxes were enhanced in association with the proton precipitation. This low-energy precipitation could be secondary electrons that are created by proton precipitation and drive the red arc.

3. Conclusion

Using three nights of citizen scientist observations and coordinated scientific imagers and low-Earth orbiting satellites, we have presented a repeatable sequence of subauroral optical emissions during substorms. During the substorm expansion phase, green diffuse emissions emerged just equatorward of the auroral oval and moved equatorward. The green diffuse emissions were identified as proton aurora because of the presence of H_β emissions and ion precipitation. The red arc was associated with the green emissions, indicating the role of secondary electrons. The red arc in the first event also had a ray structure, which also indicates the presence of low-energy precipitation. The low-Earth orbiting satellite observations provided direct evidence of low-energy secondary electron precipitation over the red arc.

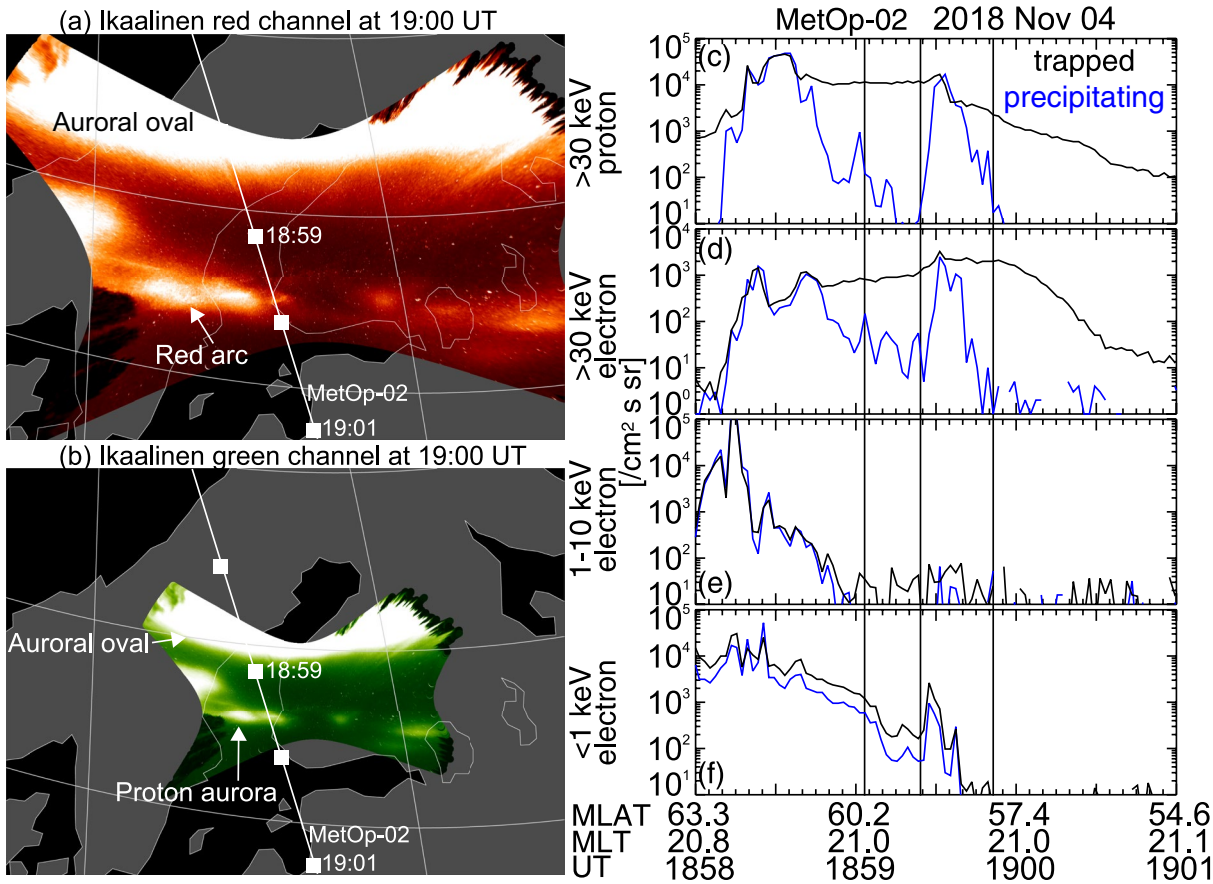

Figure 9. (Left) Snapshot of imager data in the red and green channels at 19:00 UT and the footprints of the MetOp-01 and MetOp-02 satellites. (Right) MetOp-02 measurements of the >30 keV proton, >30 keV electron, 1–10 keV electron, and <1 keV electron fluxes.

The green emissions decayed faster than the red arc, and then the red arc was recognized as a SAR arc. This transition suggests that the SAR arc is initiated by secondary electrons associated with proton precipitation. The first event shows that the secondary electrons could continue over the SAR arc after the decay of the proton aurora. Low-energy electrons are generally not observed over SAR arcs, but secondary electrons may be energetic enough only during the proton aurora and then may decrease energy below instrument coverage (i.e., transition to thermal heat flux). Collisional (Joule) heating by SAPS flows could also be the heat source for the SAR arc. The presence of proton aurora ahead of the SAR arc provides an observational support to the scenario that ion injection to the inner magnetosphere is the energy source for the SAR arc.

The present study was motivated by the citizen-scientist photographs that exhibit optical features drastically different from the classical behavior of proton aurora and SAR arcs. Similar to the research on STEVE and dunes, citizen scientists have made critical contributions to unveil the new understanding of proton aurora and SAR arcs that scientists were not aware of. We believe that observations by citizen scientists will remain important for making more discoveries of auroral physics.

Data Availability Statement

The citizen scientist images are available at https://www.amazingsky.com/Auroras/Auroras-Alberta-Saskatchewan/, https://www.taivaanvahti.fi/observations/show/51300 and https://www.taivaanvahti.fi/observations/show/79139 as image files. The TREx, CARISMA magnetometer, SuperDARN, DMSP, and NOAA data were obtained through https://data.phys.ucalgary.ca/sort_by_project/TREx/ (RGB and spectrograph CDF), https://www.carisma.ca/carisma-data-repository (ascii), http://vt.superdarn.org/tiki-index.php?page=Examine%20Fit%20Contents (fitacf), www.openmadrigal.org (DMSP), and satdat.ngdc.noaa.gov/sem/poes/data/raw/ngdc/ (daily NCDF).

Acknowledgments
This work was supported by NASA grant 80NSSC18K0657, 80NSSC20K0604, 80NSSC20K0725, 80NSSC21K1321 and 80NSSC19K0546, NSF grant AGS-1907698 and AGS-2100975, and AFOSR grant FA9559-16-1-0364. Operation of the SuperDARN radars at the Fort Hays Kansas site is supported by NSF award AGS-1935110. We thank ISSI/ISSJ-BJ for the "Multi-Scale Magnetosphere-Ionosphere-Thermosphere Interaction" and "Magnetotail Dipolarizations: Archimedes Force or Ideal Collapse?" teams. We also thank Finnish Astronomical Association Ursa for maintaining Taivaanvahti/Skywarden (https://www.taivaanvahti.fi/) service and its aurora observers. For observation-related discussions, we wish to thank Minna Glad, Matti Helin, Virpi Kauko, Raija Kokkola, Toni Korhonen, Pirjo Koski, Donna Lach, Arto Oksanen, Minna Palmroth, Pauli Sorsakari, Matias Takala, Anssi Toivanen and Rami Valonen, as well as always inspiring Facebook groups Revontulikyttääjät ("Aurora Stalkers") and Alberta Aurora Chasers.

References

Donovan, E., Mende, S. B., Jackel, B., Syrjäsuo, M., Meurant, M., Voronkov, I., et al. (2006). The azimuthal evolution of the substorm expansive phase onset aurora. In M. Syrjäsuo & E. Donovan (Eds.), *Proceedings of the Eighth International conference on substorms* (pp. 55–60). University of Calgary.

Egeland, A., & Burke, W. J. (2019). Auroral hydrogen emissions: A historic survey. *Geo Space Science*, *10*(1), 201–213. https://doi.org/10.5194/hgss-10-201-2019

Foster, J. C., Buonsanto, M. J., Mendillo, M., Nottingham, D., Rich, F. J., & Denig, W. (1994). Coordinated stable auroral red arc observations: Relationship to plasma convection. *Journal of Geophysical Research*, *99*(A6), 11429–11439. https://doi.org/10.1029/93JA03140

Gallardo-Lacourt, B., Frey, H. U., & Martinis, C. (2021). Proton aurora and optical emissions in the subauroral region. *Space Science Reviews*, *217*(1), 10. https://doi.org/10.1007/s11214-020-00776-6

Gillies, D. M., Liang, J., Donovan, E., & Spanswick, E. (2020). The apparent motion of STEVE and the Picket Fence phenomena. *Geophysical Research Letters*, *47*(20), e2020GL088980. https://doi.org/10.1029/2020gl088980

Henderson, M. G. (2021). Key elements of auroral substorm development and their relationship to recent observations of detached sub-auroral phenomena including STEVE-like emissions. *Journal of Atmospheric and Solar-Terrestrial Physics*, *218*, 105600. https://doi.org/10.1016/j.jastp.2021.105600

Inaba, Y., Shiokawa, K., Oyama, S., Otsuka, Y., Connors, M., Schofield, I., et al. (2021). Multi-event analysis of plasma and field variations in source of stable auroral red (SAR) arcs in inner magnetosphere during non-storm-time substorms. *Journal of Geophysical Research: Space Physics*, *126*(4), e2020JA029081. https://doi.org/10.1029/2020ja029081

Lummerzheim, D., Galand, M., Semeter, J., Mendillo, M. J., Rees, M. H., & Rich, F. J. (2001). Emission of OI(630 nm) in proton aurora. *Journal of Geophysical Research*, *106*(A1), 141–148. https://doi.org/10.1029/2000JA002005

MacDonald, E. A., Donovan, E., Nishimura, Y., Case, N. A., Gillies, D. M., Gallardo-Lacourt, B., et al. (2018). New science in plain sight: Citizen scientists lead to the discovery of optical structure in the upper atmosphere. *Science Advances*, *4*(3), eaaq0030. https://doi.org/10.1126/sciadv.aaq0030

Mendillo, M., Finan, R., Baumgardner, J., Wroten, J., Martinis, C., & Casillas, M. (2016). A stable auroral red (SAR) arc with multiple emission features. *Journal of Geophysical Research: Space Physics*, *121*(10), 10564–10577. https://doi.org/10.1002/2016JA023258

Montbriand, L. E. (1971). The proton aurora and auroral substorm. In B. M. McCormac (Ed.), *The radiating atmosphere* (pp. 366–373). Reidel Publishing Company.

Nishimura, Y., Bortnik, J., Li, W., Lyons, L. R., Donovan, E. F., Angelopoulos, V., & Mende, S. B. (2014). Evolution of nightside subauroral proton aurora caused by transient plasma sheet flows. *Journal of Geophysical Research: Space Physics*, *119*(7), 5295–5304. https://doi.org/10.1002/2014JA020029

Nishimura, Y., Yang, J., Pritchett, P. L., Coroniti, F. V., Donovan, E. F., Lyons, L. R., et al. (2016). Statistical properties of substorm auroral onset beads/rays. *Journal of Geophysical Research: Space Physics*, *121*(9), 8661–8676. https://doi.org/10.1002/2016JA022801

Ono, T., Hirasawa, T., & Meng, C. I. (1987). Proton auroras observed at the equatorward edge of the duskside auroral oval. *Geophysical Research Letters*, *14*(6), 660–663. https://doi.org/10.1029/gl014i006p00660

Oyama, S., Shinbori, A., Ogawa, Y., Kellinsalmi, M., Raita, T., Aikio, A., et al. (2020). An ephemeral red arc appeared at 68° MLat at a pseudo breakup during geomagnetically quiet conditions. *Journal of Geophysical Research: Space Physics*, *125*(10), e2020JA028468. https://doi.org/10.1029/2020ja028468

Palmroth, M., Grandin, M., Helin, M., Koski, P., Oksanen, A., Glad, M. A., et al. (2020). Citizen scientists discover a new auroral form: Dunes provide insight into upper atmosphere. *AGU Advances*, *1*, e2019AV000133. https://doi.org/10.1029/2019av000133

Sakaguchi, K., Miyoshi, Y., Spanswick, E., Donovan, E., Mann, I. R., Jordanova, V., et al. (2012). Visualization of ion cyclotron wave and particle interactions in the inner magnetosphere via THEMIS-ASI observations. *Journal of Geophysical Research*, *117*(A10), A10204. https://doi.org/10.1029/2012JA018180

Takagi, Y., Shiokawa, K., Otsuka, Y., Connors, M., & Schofield, I. (2018). Statistical analysis of SAR arc detachment from the main oval based on 11-year, all-sky imaging observation at Athabasca, Canada. *Geophysical Research Letters*, *45*(21), 11539–11546. https://doi.org/10.1029/2018gl079615